Conference on Modelling Fluid Flow (CMFF'22)
The 18th International Conference on Fluid Flow Technologies
Budapest, Hungary, August 30-September 2, 2022

Stability analysis of a streaky boundary layer generated by Miniature Vortex Generators

András SZABÓ[1], Péter Tamás NAGY[2], Maarten VANIERSCHOT[3] György PAÁL[2],

[1] Corresponding Author. Department of Hydrodynamic Systems, Faculty of Mechanical Engineering, Budapest University of Technology and Economics. Bertalan Lajos u. 4 - 6, H-1111 Budapest, Hungary. E-mail: aszabo@hds.bme.hu
[2] Department of Hydrodynamic Systems, Faculty of Mechanical Engineering, Budapest University of Technology and Economics.
[3] Group T Leuven Campus, Department of Mechanical Engineering, KU Leuven.

ABSTRACT

Delaying laminar-turbulent transition is an attractive method to reduce friction drag on streamlined bodies. In the case of natural transition, in which turbulence is triggered by the growth of two-dimensional Tollmien-Schlichting (TS) instabilities, this growth of the TS instabilities can be attenuated by introducing steady streamwise streaks into the boundary layer. These streamwise streaks are generated by streamwise vortices, which rearrange the flow via the lift-up mechanism. Such streamwise vortices can be induced by so-called Miniature Vortex Generators (MVGs). Although recently considerable attention has been devoted to the investigation of MVGs, and multiple studies investigated MVGs with different parameters, there is still no large-scale parameter study available in the literature. This study aims at (partially) fulfilling this knowledge gap. The methodology of Martín & Paredes (Theor. Comput. Fluid Dyn. 31, 505–517 (2017)) is followed in the calculations. First, the economic solution of the governing equations is discussed. Then, the streak amplitude, the growth factors of the TS-waves and shear-layer instabilities, which potentially lead to premature breakdown of the streaks are analysed in detail.

Keywords: Boundary layer, flow stability, Boundary Region Equation, Parabolized Stability Equations, Miniature Vortex Generators

NOMENCLATURE

Subscripts and Superscripts
Abbrevations

$\mathbf{U} = (U, V, W)$	$[-]$	base flow velocity
P	$[-]$	base flow pressure
$\mathbf{u}' = [u', v', w']^T$	$[-]$	perturbation velocity
p'	$[-]$	perturbation pressure
Re	$[-]$	Reynolds number
$\hat{\delta}$	$[m]$	boundary layer scale
$\hat{U}_0$	$[m/s]$	free-stream velocity
$\hat{\nu}$	$[m^2/s]$	kinematic viscosity
$\mathbf{q} = [u, v, w, p]^T$	$[-]$	perturbation shape function

α	$[-]$	streamwise wavenumber
ω	$[-]$	angular frequency
F	$[-]$	nondimensional frequency
$\hat{\Lambda}$	$[mm]$	MVG spanwise periodicity
$\hat{d}$	$[mm]$	MVG pair distance
$\hat{w}$	$[mm]$	MVG width
$\hat{h}$	$[mm]$	MVG height
$\hat{L}$	$[mm]$	MVG length
$\hat{L}_0$	$[mm]$	characteristic length
$\hat{x}_0$	$[mm]$	start of the computational domain
$\hat{x}_{MVG}$	$[mm]$	location of the MVG
$\hat{x}_{st}$	$[mm]$	start of the stability calculation
$\hat{\delta}_{99}$	$[mm]$	boundary layer thickness
A	$[-]$	streak amplitude
Re_δ	$[-]$	boundary layer scale Reynolds number

1. INTRODUCTION

Delaying laminar-turbulent transition over streamlined aerodynamic bodies has been an actively researched field for a long time. There are two main categories of the transition scenario: transition due to boundary layer instability and bypass transition [1]. In the former case, the boundary layer transition occurs due to the exponential amplification of small-amplitude disturbances, which can be appropriately described by linear theory. After the disturbance amplitude reaches a certain threshold, nonlinear effects set in; this is the secondary instability phase, which covers a much smaller spatial extension of the linear instability [2]. Several instability mechanisms exist; in the case of an incompressible two-dimensional boundary layer with small-to-none surface curvature, the dominant instability mechanism is the two-dimensional Tollmien-Schlichting (TS) wave. This is a well-understood, classical instability mechanism. The dampening of the TS

$\hat{\square}$ dimensional quantities
$\tilde{\square}$ variables with boundary layer scaling

MVG	Miniature Vortex Generator
BRE	Boundary Region Equations
PSE	Parabolized Stability Equations
fGMRES	flexible Generalized Minimal Residual Method

waves is the main interest of our research. The previously described instability-amplification scenario is only valid in the case of low background disturbance, i. e. turbulence intensity. In the case of high-level free-stream turbulence, instead of the slow, linear disturbance amplification, fast, nonlinear transition can occur whose mechanism can be manifold and partly poorly understood and which is termed bypass transition. However, in the first stage of the investigation of boundary-layer modification techniques to achieve drag reduction by transition-delay, always a low external disturbance level is assumed.

Several control techniques exist to modify the flow so that transition is postponed downstream. A promising method to attenuate the TS waves is the introduction of periodically varying slow-fast regions, so-called streamwise streaks into the boundary layer. It was shown both in numerical [3] and laboratory experiments [4] that with properly generated streaks, TS waves can be dampened. The physical mechanism of the TS wave attenuation is also clear: the spanwise shear generated by the streaks in the boundary layer is responsible for decreasing the disturbance energy growth [3]. Generally, the higher the streak amplitude, the higher this stabilization [3]. However, a too high streak amplitude is not desirable since then streaks become themselves unstable to inviscid secondary sinuous instabilities, which can result in an early breakdown to turbulence.

Streaks in a boundary layer can be generated in several ways. A promising passive technique was reported by Shahinfar et al.[5]: using winglet-type miniature vortex generators (MVGs), strong streaks can be generated; therefore, effective stabilization of the boundary layer can be achieved while the streaks remain stable. Following experimental studies [6, 7, 8, 9, 10] report additional information regarding the MVGs, such as: how changing a single parameter of the MVGs independently affect the boundary layer; using a second MVG row the streaks that decay downstream can be reinforced; the instability growth in the near-field of the MVGs, and also further downstream; the effect of the pressure gradient. Furthermore, the stabilization of the TS waves [9] and oblique disturbances [11] were also observed experimentally in a streaky boundary layer introduced by MVGs. In most of these studies, triangular MVGs were used, except for the investigations of Sattarzadeh et al. [9] and Sattarzadeh and Fransson [12], who examined rectangular MVGs. Interestingly, in some cases, rectangular MVGs were able to produce stronger streaks than triangular ones. Furthermore, the stronger streaks remained stable. Therefore, it can be concluded that the previous experimental studies have well established that MVGs are able to successfully generate a streaky boundary layer in which the growth of the TS waves is attenuated.

The numerical investigation of streaky boundary layers has received much less attention. Bagheri and Hanifi [13] used nonlinear Parabolized Stability Equations (PSE) to investigate the optimal spacing of the streaks to suppress TS waves. Later, Siconolfi et al. [14] used direct numerical simulation to calculate the flow around an MVG and BiGlobal stability analysis to calculate the instability modes. They obtained a reasonable agreement with the experiments. They identified several instability modes in the downstream vicinity of the MVGs, which cause local disturbance growth that might result in a premature transition to turbulence. Siconolfi et al. [15] substituted the effect of MVGs with streamwise vortices and showed that vortices placed outside the boundary layer can be much more effective for streak generation than vortices inside the boundary layer, therefore such vortices might lead to better transition delay. However, the practical generation of such vortices remains an open question.

Parallel to these numerical studies, Martín and Paredes [16] proposed a computationally effective numerical method to assess the stability of streaky boundary layers. They calculated the evolution of streaks with Boundary Region Equations (BRE), which are the extensions of the boundary layer equations: the boundary layer scaling is applied in both the wall-normal and spanwise direction. The evolution of the disturbances in the streaky boundary layer is calculated with linear PSE, which accounts for both non-local and non-parallel effects. The initial disturbances are calculated using BiGlobal stability equations. They modeled the effect of the vortex generators with Rankine vortices that have a fixed maximum amplitude, and obtained similar results to the ones of Siconolfi et al. [15, 14], verifying the validity of their approach. Later, Martín and Paredes [17] examined optimal streaks disturbances with limited maximum amplitude. They found the spanwise wavenumber and the maximum amplitude of the boundary layer streaks both have a significant influence not only on the attenuation of the TS waves but also on the sinuous instability modes. Furthermore, they predicted the transition location using the e^N method.

The above discussion illustrates that there are several topics that need to be addressed before the MVGs can be applied to commercial use. The present paper reports some initial results of our research to investigate MVGs from several different aspects. We discuss the efficient numerical implementation of the model equations used by Martín and

Paredes [16]. Then, we examine the stability of triangular and rectangular MVGs and compare the differences.

2. THEORETICAL FRAMEWORK

We investigate an incompressible zero pressure gradient flat-plate boundary layer. The nondimensional forms of the governing equations are used. Let x, y and z be the streamwise, wall-normal and spanwise coordinates respectively. Small-amplitude perturbations are considered around an equilibrium base flow. Let $\mathbf{U} = [U, V, W]^T$ and P denote the base flow velocity and pressure, and $\mathbf{u}' = [u', v', w']^T$ and p' the velocity and pressure of the small-amplitude perturbations. Then, the governing equations of the base flow are

$$\frac{\partial \mathbf{U}}{\partial t} + (\mathbf{U}\cdot\nabla)\mathbf{U} = -\nabla P + \frac{1}{\mathrm{Re}}\Delta\mathbf{U}, \tag{1}$$

$$\nabla\cdot\mathbf{U} = 0. \tag{2}$$

Furthermore, the linearised Navier-Stokes equations that describe the perturbations are

$$\frac{\partial \mathbf{u}'}{\partial t} + (\mathbf{U}\cdot\nabla)\mathbf{u}' + (\mathbf{u}'\cdot\nabla)\mathbf{U} = -\nabla p' + \frac{1}{\mathrm{Re}}\Delta\mathbf{u}', \tag{3}$$

$$\nabla\cdot\mathbf{u}' = 0. \tag{4}$$

Equations (1-4) are nondimensionalised with the free-stream velocity $\hat{U}_0$ and boundary layer length scale $\hat{\delta}_0 = \sqrt{\hat{L}_0\hat{\nu}/\hat{U}_0}$, where $\hat{\nu}$ is the kinematic viscosity, $\hat{L}_0$ is distinguished streamwise location (defined later) measured from the leading edge; dimensional variables are denoted with $\hat{\square}$. $\mathrm{Re} = \hat{\delta}_0\hat{U}_0/\hat{\nu}$ is the Reynolds number. The nondimensional pressure is $P = \hat{P}/(\hat{\rho}\hat{U}_0^2)$.

Eqs. (1-2) need to be used to describe the stationary equilibrium flow field near the MVG, since there the flow rapidly varies in all three spatial dimensions. However, after some distance downstream of the MVG, the flow-field obeys the boundary layer scaling: the flow varies slowly in the streamwise direction, while it varies more rapidly in the wall-normal and spanwise directions. Furthermore, the spanwise and wall-normal velocities can be assumed to be smaller than the streamwise velocity. Therefore, Eqs. (1-2) can be simplified by using a different nondimensionalization for the different variables. Introducing $\varepsilon = 1/\sqrt{\hat{L}_0\hat{U}_0/\hat{\nu}}$, $[\tilde{X}, \tilde{Y}, \tilde{Z}]^T = [\hat{x}/\hat{L}_0, \hat{y}\varepsilon/\hat{L}_0, \hat{z}\varepsilon/\hat{L}_0]^T$, $[\tilde{U}, \tilde{V}, \tilde{W}]^T = [\hat{U}/\hat{U}_0, \hat{V}\varepsilon\hat{U}_0, \hat{W}\varepsilon/\hat{U}_0]^T$ and $\tilde{P} = \hat{P}\varepsilon^2/(\hat{\rho}\hat{U}_0^2)$, we get

$$\tilde{U}\frac{\partial\tilde{U}}{\partial\tilde{X}} + \tilde{V}\frac{\partial\tilde{U}}{\partial\tilde{Y}} + \tilde{W}\frac{\partial\tilde{U}}{\partial\tilde{Z}} = \frac{\partial^2\tilde{U}}{\partial\tilde{Y}^2} + \frac{\partial^2\tilde{U}}{\partial\tilde{Z}^2}, \tag{5}$$

$$\tilde{U}\frac{\partial\tilde{V}}{\partial\tilde{X}} + \tilde{V}\frac{\partial\tilde{V}}{\partial\tilde{Y}} + \tilde{W}\frac{\partial\tilde{V}}{\partial\tilde{Z}} = -\frac{\partial\tilde{P}}{\partial\tilde{Y}} + \frac{\partial^2\tilde{V}}{\partial\tilde{Y}^2} + \frac{\partial^2\tilde{V}}{\partial\tilde{Z}^2}, \tag{6}$$

$$\tilde{U}\frac{\partial\tilde{W}}{\partial\tilde{X}} + \tilde{V}\frac{\partial\tilde{W}}{\partial\tilde{Y}} + \tilde{W}\frac{\partial\tilde{W}}{\partial\tilde{Z}} = -\frac{\partial\tilde{P}}{\partial\tilde{Z}} + \frac{\partial^2\tilde{W}}{\partial\tilde{Y}^2} + \frac{\partial^2\tilde{W}}{\partial\tilde{Z}^2}, \tag{7}$$

$$\frac{\partial\tilde{U}}{\partial\tilde{X}} + \frac{\partial\tilde{V}}{\partial\tilde{Y}} + \frac{\partial\tilde{W}}{\partial\tilde{Z}} = 0. \tag{8}$$

Eqs. (5-8) are called boundary region equations (BRE). These are essentially the extension of the boundary layer equations and are well known and were previously used for several different flow problems as discussed in [16]. These equations are parabolic, and with suitable initial- and boundary conditions well-posed. Thus, they can be marched downstream without any step size restriction. Note that the wall-normal and spanwise scalings are the same as in Eqs. (3-4) but the streamwise length scale is longer; furthermore, the wall-normal and spanwise velocities are magnified. Essentially, the appropriate stretching and scaling of the independent and dependent variables make the governing equations Reynolds number independent.

Eqs. (3-4) can be also simplified in multiple ways. When studying the convective instabilities in a boundary layer, it is reasonable to assume that the base-flow is locally parallel, i.e. the streamwise variation of the base flow is neglected ($\mathbf{U} = \mathbf{U}(y, z)$). This allows examination of the boundary layer as a series of parallel flows. Then, perturbations can be sought in the form

$$(u', v', w', p')(x, y, z, t) = (u, v, w, p)(y, z)e^{\mathrm{i}(\alpha x - \omega t)} + \text{c.c.} \tag{9}$$

In the equation above, (u, v, w, p) are the disturbance shape functions, ω is the angular frequency, α is the wavenumber, and c.c. means complex conjugate. In general, both α and ω can be complex quantities. In the case of a spatially developing flow such as a boundary layer, spatial stability analysis is appropriate, which means that ω is real, while α is complex. Therefore, the disturbance wave is assumed to be time-periodic which is periodic and exponentially growing or decaying in space. Substituting the above ansatz to Eqs. (3-4), we get

$$(\alpha^2\mathbf{A}_2 + \alpha\mathbf{A}_1 + \mathbf{A}_0)\mathbf{q} = 0, \tag{10}$$

where $\mathbf{q} = (u, v, w, p)$ and the coefficient matrices can be found in [14]. The above problem is a so-called BiGlobal spatial stability problem. Eq. (10) is a polynomial eigenvalue problem, which can be linearised (transformed to a generalised eigenvalue problem) and solved in a straightforward manner.

In the simplification of Eqs. (3-4), we can also assume that the base flow is not strictly parallel but it varies slowly in the streamwise direction. This way, the derived stability equations are still reasonably simple but they preserve more accuracy than Eq. (9). This requires us to seek the disturbances in the form

$$(u', v', w', p')(x, y, z, t) = (u, v, w, p)(x, y, z) e^{\mathrm{i}\left(\int_{x_0}^{x} \alpha(\xi)\mathrm{d}\xi - \omega t\right)} + \text{c.c.} \quad (11)$$

This form decomposes the perturbation into a slowly varying shape function and an exponential variation; furthermore, the streamwise variation of the streamwise wavenumber is also allowed. Substituting this into Eqs. (3-4), and neglecting small terms yields

$$\mathbf{A}\mathbf{q} + \mathbf{B}\frac{\partial \mathbf{q}}{\partial y} + \mathbf{C}\frac{\partial^2 \mathbf{q}}{\partial y^2} + \mathbf{D}\frac{\partial \mathbf{q}}{\partial z} + \mathbf{E}\frac{\partial^2 \mathbf{q}}{\partial z^2} + \mathbf{F}\frac{\partial \mathbf{q}}{\partial x} = 0. \quad (12)$$

where the coefficient matrices can be found in [18]. Eq. (12) is called the parabolized stability equations (PSE), and has been widely used to model flow stability phenomena [19]. There are two important things that must be addressed regarding the PSE. First, the splitting of the perturbation into a shape function and exponentially varying part (Eq. (11)) is ambiguous. The splitting can be defined in different ways [19]. Here, the most common method is utilised; namely, all the exponential growth of the shape-function is absorbed into α by enforcing

$$\int\int \mathbf{q}\frac{\partial \mathbf{q}}{\partial x}\mathrm{d}y\mathrm{d}z = 0 \quad (13)$$

in each marching step. Furthermore, Eq. (12) are ill-posed, because the equations are only partially parabolized but not fully parabolic. This means that there might be solutions that are traveling upstream, opposite to the marching direction, which can cause numerical instabilities. As a partial remedy, we employ the stabilization method proposed by Andersson et al. [20].

2.1. Solution of the full problem

The theoretical framework outlined in the previous section allows us to study the stability characteristics of MVGs rather efficiently. First, Eqs. (1-2) are solved as a stationary problem to obtain the flow field near the MVG. This is carried out using the commercial CFD software Fluent - details of these calculations are reported in a different CMFF22 conference paper [21]. This region is denoted by the brown box in Fig. 1. Then, BRE (Eqs. 5-8) are solved to calculate the evolution of the streaky boundary layer. This region is marked with the blue box in Fig. 1. The BRE are solved starting upstream of the downstream boundary of the 3D CFD calculation: this way the no-stress boundary condition used in the outlet of the CFD calculation does not contaminate the solution. This location is denoted with x_{st}, as this is where the stability calculation also begins. Furthermore, all equations were made nondimensional using the boundary layer length scale at this location; therefore, $\hat{L}_0 = \hat{x}_{st}$. PSE is solved after the base-flow is obtained with BRE. The initial condition for the PSE is determined by solving the BiGlobal stability problem (Eq. (10)).

The following boundary conditions were used in the problem solution. For the CFD calculation near the MVG, the inlet boundary condition is the Blasius velocity profile corresponding to the streamwise location on a theoretical flat plate. In the free-stream, a constant streamwise velocity was prescribed. In the spanwise direction, periodicity was assumed, and a no-slip boundary condition was prescribed on the bottom wall. The boundary conditions are the same for the BRE. For both the BiGlobal stability equations and PSE, periodicity was assumed in the spanwise direction, and disturbances are enforced to vanish in both the free-stream and also on the wall.

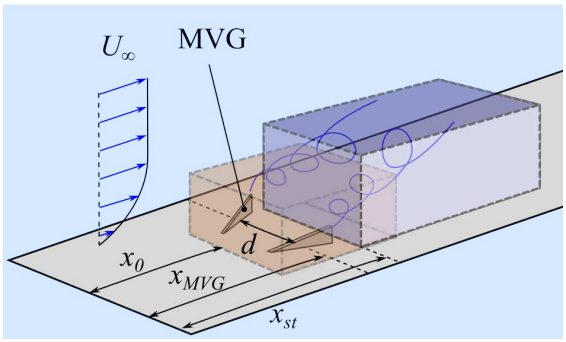

Figure 1. Sketch of the flow configuration

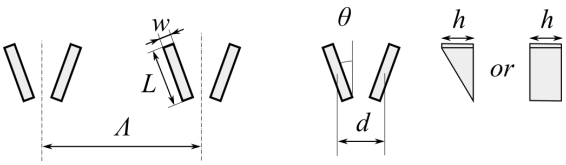

Figure 2. Parameters of the vortex generators

2.2. Parameters of the investigated configuration

The key parameters of the investigated MVG are displayed in Fig. 2 and their numerical values can be found in Table 1; these are the same as in the case investigated in [14]. The key difference in this study is that (i) not only triangular but also rectangular MVGs are considered, and (ii) the streamwise location of the MVG is varied. The different locations of the start of the computational domain, the location of the MVG, and the start of the stability calculation can be found in Table 2. These locations correspond to a flat plate with a leading edge at $x = 0$. Therefore, this also defines the boundary condition for the CFD calcula-

tion near the MVG, which then determined the initial condition of the BRE. The free-stream velocity and kinematic viscosity in this study were $\hat{U}_0 = 7.7$ m/s and $\hat{\nu} = 1.4607 \cdot 10^{-5}$ m^2/s, respectively.

Table 1. Parameters of the MVGs

$\hat{\Lambda}$ (mm)	$\hat{d}$ (mm)	$\hat{h}$ (mm)	$\hat{w}$ (mm)	$\hat{L}$ (mm)	Θ (°)
13	3.25	1.3	0.3	3.25	15

Table 2. Location of the MVGs

$\hat{x}_0$ (mm)	$\hat{x}_{MVG}$ (mm)	$\hat{x}_{st}$ (mm)	$\hat{\delta}_{99}(x_0)$ (mm)
36.95	45.95	58.95	1.3
147.80	156.79	169.79	2.6
230.93	239.93	252.93	3.25

3. NUMERICAL TECHNIQUES

The weak form of the BRE, BiGlobal stability equations and PSE are solved using the open-source finite element software FreeFem [22]. Meshes consisting of 12000 – 15000 triangles were used in the present study which were generated using the mesh generator software BAMG that is integrated with FreeFem. The equations were discretised using $\mathcal{P}_2$ elements for the velocity fields and $\mathcal{P}_1$ elements for the pressure, which together are often referred to as the classical Taylor-Hood discretization method. The parallel version of FreeFem was used: the computational domain was decomposed into multiple parts, and each part is assigned to a single process, which allows using effective distributed-memory algorithms.

The PETSc and SLEPc packages were used to solve the linear/nonlinear equations and the polynomial eigenvalue problem, respectively. The BRE marching procedure requires a solution of a nonlinear problem in each spatial step, which was carried out using an implementation of the Newton method in PETSc. The BiGlobal polynomial eigenvalue problem was transformed using the companion-matrix method [23] in combination with a shift-invert spectral transformation which allows the calculation of the eigenvalues near a prescribed target. The eigenvalues of the transformed system were calculated using the Krylov-Schur method. Finally, the PSE, which is also nonlinear due to the constraint of Eq. (13), was solved using a straightforward fixed-point iteration [19].

The BRE, BiGlobal and PSE equations all require the solution of linear systems of equations. Generally, this is carried out by calculating the LU factorization of the system matrix. This was also the main method utilised in the present study using the external library MUMPS. However, the PETSc library is primarily designed to solve sparse linear systems using iterative methods; this enables us to use a more efficient solution technique to solve the BRE and PSE problems, which require the repeated solution of linear equations in each marching step. The PETSc library always solves preconditioned linear systems with iterative methods:

$$\mathbf{Ax} = \mathbf{b} \rightarrow \mathbf{AP}^{-1}\mathbf{y} = \mathbf{b},\ \mathbf{y} = \mathbf{Px}. \tag{14}$$

Here, $\mathbf{P}$ is the preconditioner matrix. In the case of a direct solver, the preconditioner should be $\mathbf{P} = \mathbf{A}$, and in each marching step, the system matrix, the preconditioner, and its inverse are all calculated repeatedly during the iteration. However, it is possible that the preconditioner is not updated after the first iteration:

$$\mathbf{A}_0\mathbf{A}_0^{-1}\mathbf{y}_0 = \mathbf{b}_0, \tag{15}$$

$$\mathbf{A}_1\mathbf{A}_0^{-1}\mathbf{y}_1 = \mathbf{b}_1. \tag{16}$$

Then, in the second iteration, the system is only approximately solved by the preconditioner. However, as the new system matrix $\mathbf{A}_1\mathbf{A}_0^{-1}$ is relatively close to the identity matrix, it can be solved using iterative methods. This can speed up the calculation significantly, since calculating an LU factorization is computationally demanding even for moderate systems as in the present study. Calculating the LU factorization only once and then using the flexible-GMRES (fGMRES) method (which is readily available in PETSc) for the rest of the iterations in each marching step, we managed to achieve significant computational speedup, which is reported in the next section.

4. RESULTS

4.1. Computational time

Here, we report the computational time for the simulation of the sinuous instability mode in a boundary layer perturbed by idealised Rankine vortices. Such a configuration mimics the effect of the MVGs and was previously studied in the literature [15, 16]. The presented case corresponds to the configuration *E1* studied by [16], which was also used to validate our codes. All the present calculations were carried out on a machine with an AMD Ryzen 9 3900X processor. FreeFem version 4.10 was compiled and run on a virtual machine with Ubuntu 18.04 mounted using Oracle Virtualbox under Windows.

Fig. 3 displays the computational time for solving the BRE equations. Two regions with different scaling can be identified: using 2-4 cores, the computational time decreases fast with increasing the number of cores; then, increasing the number of cores further the scaling falls off. This can be attributed to the fact that the problem size is relatively small. Interestingly, when using 4-10 cores, using an odd number of processes seems advantageous since with even cores the computational time reduction is lower. Comparing LU factorization and fGMRES, the iterative solver outperforms the direct solution procedure significantly: the computational time is reduced by approximately a factor of 0.5 using the iterative solver.

Fig. 4 is the same as Fig. 3 but for the PSE equa-

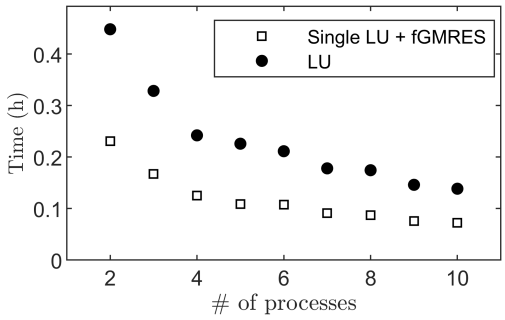

Figure 3. Comparison of the different techniques to solve the linear system of equations, BRE equations

tions. Similar trends can be observed as in the case of BRE, except that the computational time is reduced only by a factor of ≈ 0.4 with the use of the iterative method. This is likely because the solution of the linear system of equations takes up a smaller portion of the PSE calculation. Nevertheless, the computational time decrease is quite significant. Note that the solution of the PSE equations takes significantly more time due to two reasons: (i) here, the equations are complex, and (ii) PSE need to be solved for several frequencies to obtain a complete stability map. Therefore, the decrease of computational time can be considered significant.

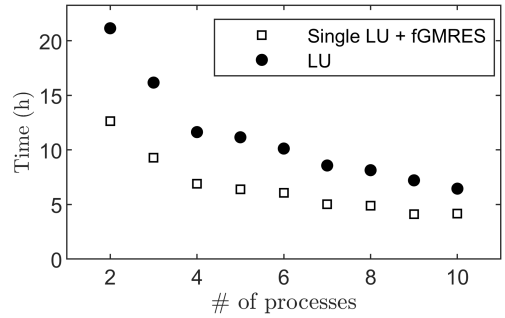

Figure 4. Comparison of the different techniques to solve the linear system of equations, PSE equations

4.2. Stability characteristics of the MVGs

First, results for the streak amplitude generated by the MVGs are reported. The streak amplitude is measured using the formula proposed by Shahinfar et al. [7]:

$$A(x) = \frac{1}{\hat{U}_0} \int_{-0.5}^{0.5} \int_{0}^{\eta^*} \left| \hat{U}(x,\eta,\zeta) - \hat{U}^z(x,\eta) \right| \mathrm{d}\eta \mathrm{d}\zeta, \tag{17}$$

where $\eta = \hat{y}/\hat{\delta}(\hat{x})$, $\zeta = \hat{z}/\hat{\Lambda}$, and U^z is the spanwise average of the streamwise velocity. η^* is a sufficiently high location so that the the free-stream is undisturbed, i.e., the integrand of Eq. 17 vanishes. The streak amplitude is displayed in Figs. 5 and 6 as a function of the nondimensional streamwise coordinate Re_δ in the case of triangular and rectangular MVGs with different positions along the flat plate. It is apparent from the comparison that rectangular MVGs generate stronger vortices than triangular ones for the same MVG height and streamwise position. It can be also deduced that moving the MVG upstream results in the generation of a stronger streak. For $\hat{\delta}_{99} = 2.6$ and 3.25 mm the variation of the amplitude has the same structure: a fast initial increase followed by a slow decay. However, for $\hat{\delta}_{99} = 1.3$ mm the amplitude variation has an oscillatory character, and these streaks are much stronger and more persistent. This is because the increased relative height results in a stronger amplitude and also because vortices close to the edge of the boundary layer are the most effective for generating streaks [15, 16]. However, these latter MVGs with strong streaks are susceptible to secondary sinuous inviscid instabilities; therefore, they are omitted in the following discussion.

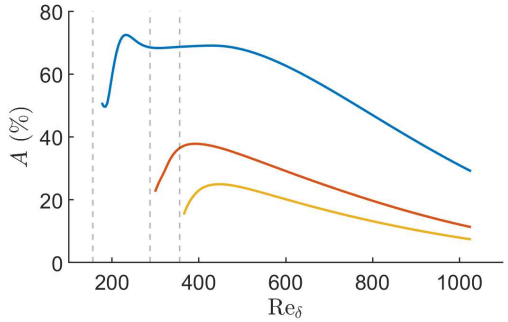

Figure 5. Integral streak amplitude in the case of triangular MVGs. The grey vertical dashed line denotes the location of the MVG. The blue, red and yellow lines correspond to $\hat{\delta}_{99} = 1.3, 2.6$ and 3.25 mm, respectively.

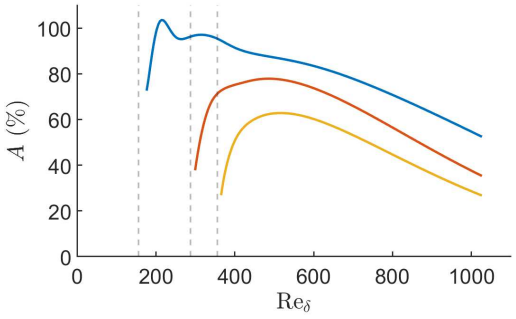

Figure 6. Integral streak amplitude in the case of rectangular MVGs. The grey vertical dashed line denotes the location of the MVG. The blue, red and yellow lines correspond to $\hat{\delta}_{99} = 1.3, 2.6$ and 3.25 mm, respectively.

Fig. 7 shows the neutral stability curves of the different instability modes for a triangular MVG with height $\hat{\delta}_{99} = 3.25$ mm, where $F = \hat{\omega}\hat{\nu}/\hat{U}_0^2 \cdot 10^6$ is the nondimensional frequency parameter. The unstable region is denoted by the shaded grey area. There are two main instability regions: the near field of the MVG ($\mathrm{Re}_\delta < 400 - 500$), where multiple instability modes exist, and the downstream region $\mathrm{Re}_\delta > 500$), where the neutral curve of the TS waves can be observed. In the case of the unstable upstream region, only the modes that form the border of the unstable region are displayed. These results are in agreement with the findings of [14] who studied a configuration is very similar to this ($\hat{\delta}_{99} = 3.12$ mm). However, the shape of the unstable region near the MVG is slightly different between the two cases. This is likely because here, PSE was used, which includes non-local and non-parallel effects, while in [14] Bi-Global stability analysis was used, which assumes a locally parallel flow and is, therefore, less accurate. In Fig. 8, the same neutral curves are displayed but the same MVG is moved further upstream so that $\hat{\delta}_{99} = 2.6$ mm. A stronger stabilization of the TS waves is observed: the unstable region is shifted upstream and also toward lower frequencies. Interestingly, the boundary of the unstable region near the MVG did not move much. However, as the MVG is moved upstream, the spatial extent of this unstable region is much larger; therefore, it is more likely that this MVG advances transition.

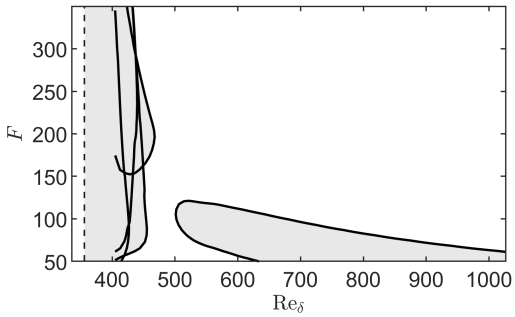

Figure 7. Neutral stability curves of the unstable eigenmodes in the streaky boundary layer. The unstable region is denoted with the shaded grey area. Triangular MVG, $\hat{\delta}_{99} = 3.25$ mm.

In the case of all rectangular MVGs investigated in this study, we found that although strong streaks are generated, and TS waves are completely suppressed, secondary sinuous modes are unstable in the region that has a large spatial extent (not shown). Therefore, the presently investigated rectangular MVG configurations likely advance transition. This finding is different than the observations of [12] and can be explained by the fact that our MVGs are larger compared to the boundary layer height than in the cited reference. These observations point out that the streak amplitude alone is not a good measure of the instability characteristic and further studies are required to assess the interaction of the MVGs with the boundary layer.

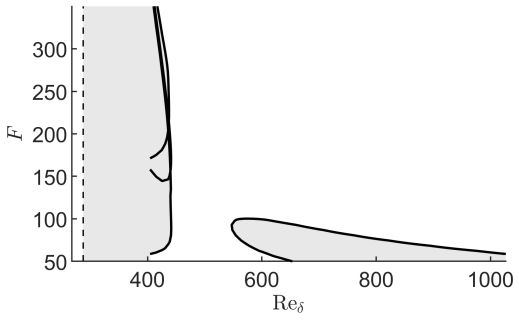

Figure 8. Neutral stability curves of the unstable eigenmodes in the streaky boundary layer. The unstable region is denoted with the shaded grey area. Triangular MVG, $\hat{\delta}_{99} = 2.6$ mm.

Finally, we note that the tracking of the individual modes was problematic in the near-field of the MVGs, especially in the case of rectangular MVGs. The reason for this is that PSE is able to track only a single eigenmode; see [24] for discussion. Therefore, for the near-wake region of the MVG, BiGlobal stability analysis might be a better tool as it can identify multiple modes in the eigenvalue spectrum.

5. CONCLUSIONS

In this paper, a short review of the research on MVGs is presented. Based on suitable approximations for the different flow regions, model equations that allow the economic solution of the problem are presented. Effective numerical solution of the equations is discussed, including an iterative method that reduces the computational cost significantly. Then, the stability of a few MVG geometries is analyzed, including rectangular MVGs, which were not considered in previous numerical studies. The results indicate that different MVG geometries can generate streaks that have remarkably different stability characteristics. Therefore, future studies should investigate the differences between different MVG geometries.

ACKNOWLEDGEMENTS

The authors would like to thank Pierre Jolivet for the help with the parallel capabilities of FreeFem and also for suggesting reusing the LU factorization as a preconditioner for iterative methods.

The work has been performed within the framework of the NKFI project K124939. The generous support of the CELSA foundation is acknowledged.

REFERENCES

[1] Kachanov, Y. S., 1994, "Physical Mechanisms of Laminar-Boundary-Layer Transition", *An-*

nual Review of Fluid Mechanics, Vol. 26, pp. 411–482.

[2] Herbert, T., 1988, "Secondary Instability of Boundary Layers", *Annual Review of Fluid Mechanics*, Vol. 20, pp. 487–526.

[3] Cossu, C., and Brandt, L., 2004, "On Tollmien-Schlichting-like waves in streaky boundary layers", *European Journal of Mechanics - B/Fluids*, Vol. 23, pp. 815–833.

[4] Fransson, J. H. M., Talamelli, A., Brandt, L., and Cossu, C., 2006, "Delaying Transition to Turbulence by a Passive Mechanism", *Physical Review Letters*, Vol. 96, p. 064501.

[5] Shahinfar, S., Sattarzadeh, S. S., Fransson, J. H. M., and Talamelli, A., 2012, "Revival of Classical Vortex Generators Now for Transition Delay", *Phys Rev Lett*, Vol. 109, p. 74501.

[6] Fransson, J. H. M., and Talamelli, A., 2012, "On the generation of steady streamwise streaks in flat-plate boundary layers", *Journal of Fluid Mechanics*, Vol. 698, pp. 211–234.

[7] Shahinfar, S., Fransson, J. H. M., Sattarzadeh, S. S., and Talamelli, A., 2013, "Scaling of streamwise boundary layer streaks and their ability to reduce skin-friction drag", *Journal of Fluid Mechanics*, Vol. 733, pp. 1–32.

[8] Sattarzadeh, S. S., Fransson, J. H. M., Talamelli, A., and Fallenius, B. E. G., 2014, "Consecutive turbulence transition delay with reinforced passive control", *Physical Review E*, Vol. 89, p. 061001.

[9] Sattarzadeh, S. S., and Fransson, J. H. M., 2014, "Experimental investigation on the steady and unsteady disturbances in a flat plate boundary layer", *Physics of Fluids*, Vol. 26, p. 124103.

[10] Downs, R. S., Fallenius, B. E. G., Fransson, J. H. M., and Mårtensson, H., 2017, "Miniature Vortex Generators for Flow Control in Falkner–Skan Boundary Layers", *AIAA Journal*, Vol. 55, pp. 352–364.

[11] Shahinfar, S., Sattarzadeh, S. S., and Fransson, J. H. M., 2014, "Passive boundary layer control of oblique disturbances by finite-amplitude streaks", *Journal of Fluid Mechanics*, Vol. 749, pp. 1–36.

[12] Sattarzadeh, S. S., and Fransson, J. H. M., 2015, "On the scaling of streamwise streaks and their efficiency to attenuate Tollmien-Schlichting waves", *Experiments in Fluids*, Vol. 56, p. 58.

[13] Bagheri, S., and Hanifi, A., 2007, "The stabilizing effect of streaks on Tollmien-Schlichting and oblique waves: A parametric study", *Physics of Fluids*, Vol. 19, p. 78103.

[14] Siconolfi, L., Camarri, S., and Fransson, J. H. M., 2015, "Stability analysis of boundary layers controlled by miniature vortex generators", *Journal of Fluid Mechanics*, Vol. 784, pp. 596–618.

[15] Siconolfi, L., Camarri, S., and Fransson, J. H., 2014, "Boundary layer stabilization using free-stream vortices", *Journal of Fluid Mechanics*, Vol. 764, pp. R21–R212.

[16] Martín, J. A., and Paredes, P., 2017, "Three-dimensional instability analysis of boundary layers perturbed by streamwise vortices", *Theoretical and Computational Fluid Dynamics*, Vol. 31, pp. 505–517.

[17] Martín, J. A., and Paredes, P., 2021, "Transition Prediction in Incompressible Boundary Layer with Finite-Amplitude Streaks", *Energies 2021, Vol 14, Page 2147*, Vol. 14, p. 2147.

[18] Paredes, P., 2014, "Advances in global instability computations: from incompressible to hypersonic flow", Ph.D. thesis, Universidad Politécnica de Madrid.

[19] Herbert, T., 1997, "Parabolized Stability Equations", *Annual Review of Fluid Mechanics*, Vol. 29, pp. 245–283.

[20] Andersson, P., Henningson, D. S., and Hanifi, A., 1998, "On a Stabilization Procedure for the Parabolic Stability Equations", *Journal of Engineering Mathematics*, Vol. 33 (3), pp. 311–332.

[21] Maarten, V., Péter Tamás, N., András, S., and Paál, G., 2022, "Direct Numerical Simulation of the Wake Flow of a Miniature Vortex Generator and its Interaction with a Laminar Boundary Layer", *to appear in: Proceedings of Conference on Modelling Fluid Flow (CMFF'22).*

[22] Hecht, F., 2012, "New development in freefem++", *Journal of Numerical Mathematics*, Vol. 20 (3-4), pp. 251–266.

[23] Bridges, T. J., and Morris, P. J., 1984, "Differential eigenvalue problems in which the parameter appears nonlinearly", *Journal of Computational Physics*, Vol. 55, pp. 437–460.

[24] Towne, A., Rigas, G., and Colonius, T., 2019, "A critical assessment of the parabolized stability equations", *Theoretical and Computational Fluid Dynamics 2019 33:3*, Vol. 33, pp. 359–382.